Reaction Mechanisms Between Molten CaF$_2$−based Slag and Molten

9CrMoCoB Steel

Lei-zhen Peng[1], *Zhou-hua Jiang*[1], *and Xin Geng*[1]

School of Metallurgy, Northeastern University, Shenyang 110819, China

Lei-zhen Peng: neuwindqishi@163.com

Zhou-hua Jiang: Corresponding author, jiangzh63@163.com

Xin Geng: gengx@smm.neu.edu.cn

Abstract: It is important to study the reaction mechanisms between slag and 9CrMoCoB in order to develop the proper ESR slag for producing the qualified ingot. In this article, the equilibrium reaction experiments between 9CrMoCoB and slag of $55\%CaF_2$–$20\%CaO$–$3\%MgO$–$22\%Al_2O_3$–$x\%B_2O_3$ (wt%) were conducted. The reaction mechanisms between 9CrMoCoB and slag were deduced and analyzed based on the compositions of the steel and slag samples at different reaction time. Results showed that when the B_2O_3 content is 0.5% and FeO content ranges from 0.018% to 0.22% in the slag, B content can be controlled within the target range. When the B_2O_3 content is $\geq$ 1%, the reaction between Si and B_2O_3 leads to the increasement of B content. The proper SiO_2 and B_2O_3 additional contents should be based on the ratio of [B] / [Si] in the electrode, and the SiO_2 addition can inhibit the reaction between Si and Al_2O_3.

Key Words: 9CrMoCoB, B_2O_3, slag, thermodynamic calculation, reaction mechanisms

1 Introduction

With the increasing awareness of environmental protection and the pursuit of a better life, it is necessary to develop the ultra-supercritical (USC) thermal power station units to improve the efficiencies of the thermal power plants, and reduce the emissions of the harmful gases [1−3]. 9CrMoCoB (COST-FB2) was developed in the framework of the European COST program by adding a certain content of B into the 9CrMoCo steel to produce the large-scale rotor forging. The soluble B in the 9CrMoCoB steel replaces carbon in $M_{23}C_6$ carbides, i.e., it forms a $M_{23}(B, C)_6$ phase, which is more resistant to coarsening than the B-free carbides at high temperature. The 9CrMoCoB steel is a promising material for service at 625 °C and 32 MPa pressure for its good creep property [4]. Under these advanced ultra-supercritical (A-USC) conditions, the efficiency of thermal power plant can increase by about 5%, and

CO_2 emission can reduce by about 10% compared with the world average at present [5−7].

The rotor is one of the most important components of steam turbine and its working condition is severe, given that, the high cleanliness and homogeneity ingot without interior defects such as non-metallic inclusion, porosity and segregation are required [8]. Electroslag remelting (ESR) is widely used for producing high quality ingots for the exclusive producing advantages [9−11], such as the secondary refining, removing the nonmetallic inclusions effectively, avoiding the segregation and shrinkage, and homogeneous distribution of elements [12−14]. Most turbine manufacturers employ the ESR process to produce a rotor ingot [15−17]. However, during the ESR of 9CrMoCoB process, the contents (wt%) of Al (less than 0.01%), Si (less than 0.1%), O (less than 0.0035%), and B (0.008%~0.011%) are difficult to be controlled within the narrow target range.

Molten slag has a major influence on the ingot contents during the ESR process [18−19]. Previous researchers have extensively studied the reactions between molten slag and steel to reduce the loss of the active element content in the ESR ingot. G. Pateisky [20], S. F. Medina [21], J. Fedko [22] and D. S. Kim [23] found that adding the components involved in the redox reaction into the molten slag could improve the homogeneity of the ingot by decreasing the degree of slag–metal reactions. Currently, few reports on ESR slag for remelting 9CrMoCoB have been published, and the production of 9CrMoCoB is still at the preliminary stage. It is primary to make the reaction mechanisms between CaF_2-based slag and molten 9CrMoCoB steel clear in order to develop the proper ESR slag for remelting the qualified 9CrMoCoB ingot.

First, the equilibrium reaction experiments between the molten slag of 55%CaF$_2$–20%CaO–3%MgO–22%Al$_2$O$_3$–x%B$_2$O$_3$ and 9CrMoCoB were conducted in this work. Then, the reaction mechanisms between the molten slag and steel were deduced and analyzed based on the experimental results. The meaningful goal of this study is to provide some theoretical guidance for the design of proper ESR slag for remelting the qualified 9CrMoCoB ingot with controlling the B, Si, Al, and O contents within the target range.

2 Experiments

During the ESR of the 9CrMoCoB process, redox reactions usually make the content of the active and main reinforced element B out of the target range, leading to the unqualified ingot. It can effectively inhibit the redox reaction by adding a certain amount of B$_2$O$_3$ into the slag of 55%CaF$_2$–20%CaO–3%MgO–22%Al$_2$O$_3$ (SiO$_2$ was the impurity and unavoidable, wt%). The slag compositions are shown in Table 1.

The slag was pre-melted using the reagent-grade powders of wt (CaO) $\geq$ 97%, wt (MgO) $\geq$ 98%, wt (CaF$_2$) $\geq$ 98.5%, wt (Al$_2$O$_3$) $\geq$ 98.5%, and wt (B$_2$O$_3$) $\geq$ 98%. The powders were mixed completely, then, put in a graphic crucible lined with a 0.2 mm-thick molybdenum film and heated in the MoSi$_2$ furnace shown in Fig. 1. During the experiment, the temperature was continuously measured using a B-type thermocouple, and the final temperature was 1723 K (1450℃). For composition homogeneity, the slags were held at 1723 K for 50 min and then furnace-cooled to room temperature. The compositions of the pre-melted slags are also shown in Table 1.

Table 1. The compositions of the slag / wt%

	Before pre-melted					After pre-melted					
	CaF_2	CaO	Al_2O_3	MgO	B_2O_3	CaF_2	CaO	Al_2O_3	MgO	B_2O_3	SiO_2
10#	55	20	22	3.0	0.0	53.10	21.32	21.83	3.10	0.00	0.15
11#	55	20	22	3.0	0.5	52.90	21.15	21.71	3.08	0.47	0.18
12#	55	20	22	3.0	1.0	52.68	21.02	21.62	3.07	0.97	0.16
13#	55	20	22	3.0	1.5	52.42	20.92	21.54	3.05	1.45	0.18
14#	55	20	22	3.0	2.0	52.18	20.79	21.43	3.03	1.94	0.15
15#	55	20	22	3.0	3.0	51.69	20.59	21.23	3.02	2.89	0.18

The equilibrium reaction experiments were conducted with 600 g 9CrMoCoB steel (the steel was smelted in Electrometallurgy Laboratory of Northeastern University using the 30 kg vacuum induction furnace and the steel contents were shown in Table 2) and 100 g pre-melted slag. The experiments were conducted in a magnesium oxide crucible lined with a 0.2 mm-thick molybdenum film at the isothermal zone of the $MoSi_2$ furnace shown in Fig. 1. The furnace was heated to pre-set 1823 K (1550℃) at a rate of 8 K.min^{-1}, and the temperature was continuously measured using a B-type thermocouple. During the experiments, pure argon began to blow from gas tube into the furnance as the protecting gas when the temperature was above 673 K (400℃). The bottom argon gas flow rate was 3 NL.min^{-1}, and the top argon gas flow rate was 6 NL.min^{-1}, the concentration of O_2 in the furnace atmosphere ranged from 0.2%~0.3% (volume fraction).
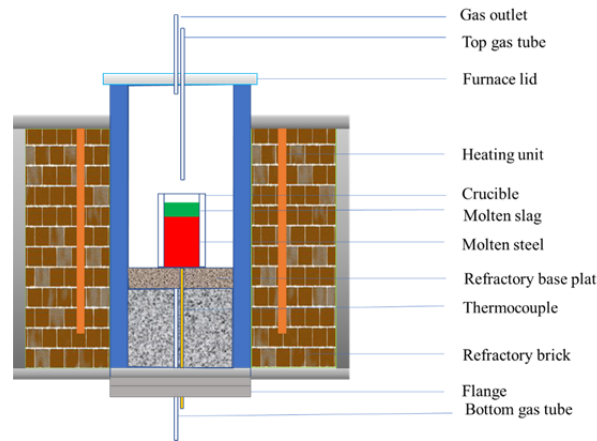
Fig. 1.   Schematic of experimental resistance furnace.

When the temperature reached 1823 K, the −0# steel sample was taken as the initial

chemical composition of 9CrMoCoB using a quartz tube. 100 g pre-melted slag was then put

into the crucible. To determine the equilibrium time of the reactions, it is necessary to take

samples at different reaction time. The reaction time began to calculate after the slag was

added (the time for adding the slag was as short as 50 s, so the time was negligible).

Subsequently, the samples of slag and steel were taken at 20, 40, and 60 min and labeled as

−1#, −2#, and −3#, respectively. The slag samples were stuck using the water-cooled copper

pipe, and the steel samples were extracted using the quartz tubes and cooled in water

immediately. To extract the steel sample, the furnace lid should be lifted away from the

furnace first, then, the quartz tube was put into the furnace to extract the steel sample from the

top of the furnace.

Table 2.   Mass percent of 9CrMoCoB / wt%

C	Si	Mn	B	Al	Cr	Mo	Co	O	Ni	Nb	N	Fe
0.136	0.0495	0.34	0.010	0.003	9.36	1.48	1.28	0.0028	0.16	0.06	0.021	Bal.

An optical emission spectrometer (ARL 4460) was used to detect the main alloying

elements in the steel samples. N, O contents in the steel samples were determined with a LECO combustion analyzer using the inert gas fusion method (LECO TC-500). The alloyed elements Al, B and Si contents and the contents of slag components were analyzed in the national analysis center for iron and steel (CISRI) using the method of ICP-AES, X-ray fluorescence spectroscopy (Rigaku ZSX Primus Ⅱ, Japan), and chemical titration.

3　Results and discussion

3.1 The results of experiments

The changes in B, Si, Al, and O contents versus time in each heat are shown in Fig. 2.
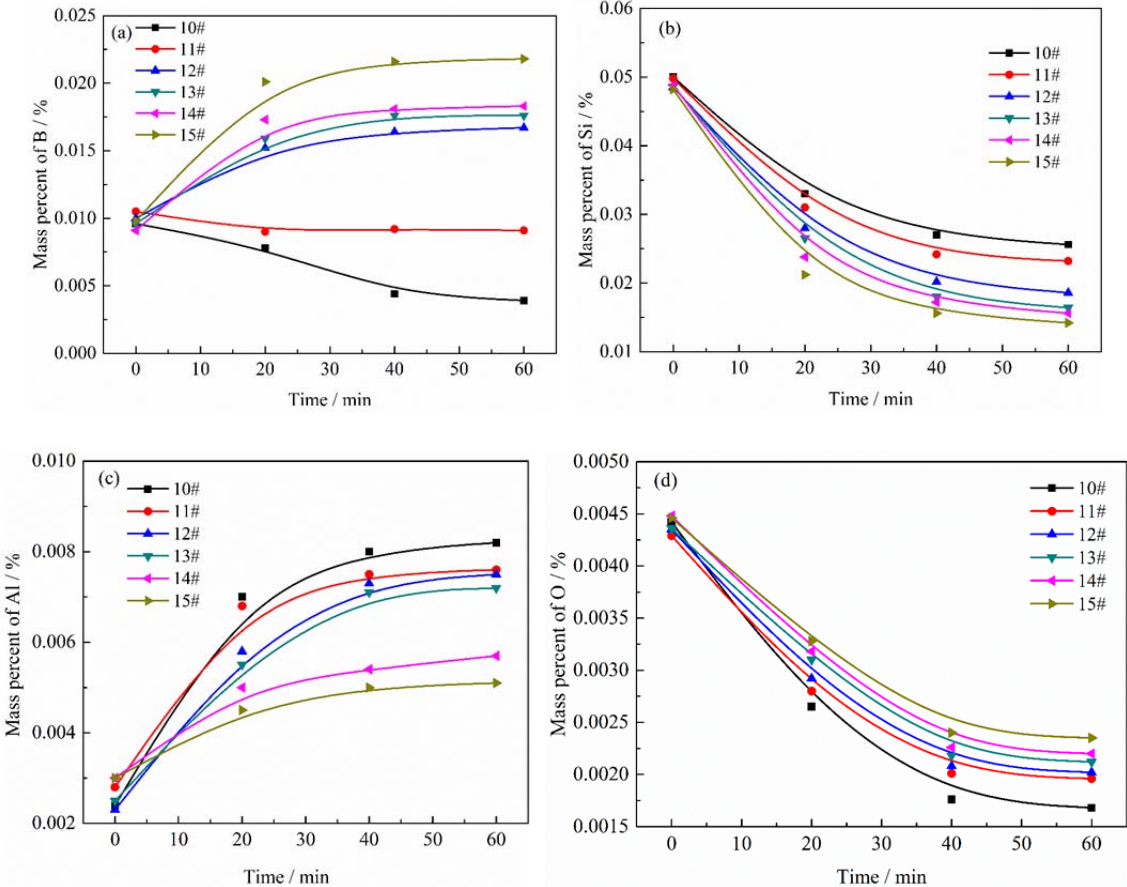
Fig. 2.　changes in the B, Si, Al and O contents, (a) boron, (b) silicon, (c) aluminum, (d) oxygen.

As shown in Fig. 2(a), for the 10# heat, the boron content gradually decreased with the reaction time. For the 11# heat, the boron content generally kept steady with a slight loss

during the whole reaction time. For the 12#–15# heats, the boron content significantly increased with the reaction time. In Fig. 2(b), the behavior of Si was different from boron. The Si content decreased with the reaction time in the six heats. In Fig. 2(c), the Al content gradually increased with the reaction time, while in Fig. 2(d), the O content decreased with the reaction time. The B, Si, Al, and O contents in all the six heats reached stable after 40 min. These results indicated that the reaction between slag and steel was in equilibrium state at 60 min. In Fig. 2(a), Fig. 2(d), the equilibrium contents of B, O at 60 min increased with the B_2O_3 addition increasing. In Fig. 2(b), Fig. 2(c), the equilibrium contents of Al, Si at 60 min decreased with the B_2O_3 addition increasing. The balanced slag compositions of each heat at 60 min are shown in Table 3.

Table 3.   The balanced slag compositions of each heat / wt%

	CaF_2	CaO	Al_2O_3	MgO	B_2O_3	SiO_2	FeO
10−3#	51.52	20.41	21.22	5.56	0.062	1.150	0.184
11−3#	51.22	20.10	21.06	5.91	0.430	1.200	0.218
12−3#	50.96	19.80	20.92	6.17	0.540	1.270	0.300
13−3#	50.72	19.30	20.76	6.13	0.810	1.320	0.324
14−3#	50.58	19.67	20.53	5.67	1.130	1.330	0.356
15−3#	50.25	20.08	20.46	6.14	1.650	1.360	0.423

3.2 The thermodynamic calculation and analysis

(1) The activities of steel and slag components

To calculate the activities of the alloyed elements in the steel, 1% mass percent was chosen as the standard state for the dilute solution activity calculation, and the model of Wagner-Chipman [24] shown below was applied.

$$a_i = f_{i(w)} \times (w_i / w^\theta) \tag{1}$$

8

$$\lg f_i = (w_i / w^\theta)e_i^i + \sum_{j \neq i}(w_j / w^\theta)e_i^j \tag{2}$$

Where the a_i is the activity of i; i is on behalf of the alloyed element in the steel; $f_{i(w)}$ is the activity coefficient of i; w_i is the mass percentage of i; e_i^i is the self−activity coefficient; e_i^j is the activity interaction coefficient. The activity interaction coefficients [25] are listed in Table 4 and the activities of the main elements are shown in Table 5.

Table 4.   Interaction coefficient of alloy elements

	Al	B	Co	Cr	Mn	Mo	N
B	-	0.038	-	-	-	-	0.074
Si	0.058	0.2	-	-0.0003	0.002	-	0.09
Al	0.045	-	-	0.012	-	-	-0.058
O	-3.9	-2.6	0.008	-0.04	-0.021	0.0035	0.057
	Nb	Ni	O	P	S	Si	C
B	-	-	-1.8	-	0.048	0.078	0.22
Si	-	-	-0.083	-0.0035	-0.048	0	0.18
Al	-	-	-6.6	-	0.03	0.0056	0.091
O	-0.14	0.006	-0.20	0.07	-0.133	-0.131	-0.45

Table 5.   The activity of the alloyed elements Al, Si, B, and O in each heat at 60 min

No.	Si	Al	B	O
10#−3	0.03007	0.01068	0.00469	0.00048
11#−3	0.02739	0.00984	0.00992	0.00055
12#−3	0.02178	0.00954	0.01777	0.00059
13#−3	0.01917	0.00917	0.01903	0.00060
14#−3	0.01831	0.00738	0.02005	0.00060
15#−3	0.01676	0.00644	0.02367	0.00067

To calculate the activities of the components in the balanced slag, the agglomerated electron phase model was used [22]. The steps for calculating the activities of slag

components were as follows:

$$a_{(i)} = X_i \Psi_i = \gamma_i (\% w_i) \tag{3}$$

$$\Psi_i^{-1} = \sum_{j=1}^{K} X_j \exp(-\zeta_{ij} / RT) \tag{4}$$

$$\zeta_{ij} = \frac{1}{2}(H_i^{1/2} - H_j^{1/2})^2 \tag{5}$$

Where the $a_{(i)}$ is the activity of i; i is on behalf of the component of the slag; X_i is the molar concentration of the atom i, %; Ψ_i is the activity coefficient of the atomic i; γ_i is the activity coefficient of i; ζ_{ij} is the exchange energy, k J.mol^{-1}; K is the total numbers of the elements in the slag system; H_i is the atomic energy scalar of the element i, k J.mol^{-1}. H_i was generated in accordance with the standard Gibbs free energy. The accurate values are shown in Table 6 [26]. The calculated activities of the main components in the balanced slag of each heat are shown in Table 7.

Table 6.   Value of H_i of the element i / k J.mol^{-1}

Ca	Si	Al	B	F	O	Mg
104.67	171.66	125.60	196.78	1545.93	1256.04	146.44

Table 7.   The activities of the main components in the balanced slag in each heat

NO.	SiO$_2$	Al$_2$O$_3$	B$_2$O$_3$/10^{-6}	FeO
10#−3	0.00073	0.03171	0.055	0.07023
11#−3	0.00083	0.03534	1.520	0.07004
12#−3	0.00082	0.03312	2.668	0.07060
13#−3	0.00088	0.03559	3.362	0.07041
14#−3	0.00090	0.03693	3.958	0.07046
15#−3	0.00093	0.03665	5.784	0.07052

(2) Analysis of the reaction between B and FeO

During the 10# heat, the B content decreased with time while the Al content increased simultaneously, the reaction between B and Al$_2$O$_3$ may occur [23].

$$2[B]+(Al_2O_3)=(B_2O_3)+2[Al] \tag{6}$$

$$\Delta G^{\ominus} = 154827 - 35.2T \tag{7}$$

$$\Delta G = 154827 - 35.2T + RT \ln \frac{a_{Al}^2 \times a_{B_2O_3}}{a_B^2 \times a_{Al_2O_3}} \qquad (8)$$

Substitution the known data into Equation (8), ΔG is positive, thus, the loss of B was not caused by the reaction between B and Al_2O_3.

The heat was not conducted in the fully sealed furnace, atmospheric oxygen can enter the furnance. A certain content of FeO in the slag was inevitable [21], which was verified by the analyzed results shown in Table 3. During the experiment process, the reaction between B and FeO may occur.

$$2[B]+3(FeO)=(B_2O_3)+3[Fe] \qquad (9)$$

$$\Delta G^{\ominus} = -478568 + 141.4T \qquad (10)$$

$$\Delta G = -478568 + 141.4T + RT \ln \frac{a_{Fe}^3 \times a_{B_2O_3}}{a_B^2 \times a_{FeO}^3} \qquad (11)$$

$$\lg[\%B] = \frac{1}{2}\lg\frac{(\%B_2O_3)}{(\%FeO)^3} + \frac{1}{2}\lg\frac{\gamma_{B_2O_3}}{\gamma_{FeO}^3} - \lg f_B - 3.167 \qquad (12)$$

Substitution the known data into Equation (11), the ΔG was negative. The reaction between B and FeO occurred.

Substitution the B_2O_3 content in the slag samples of the 10−1# (0.018%), 10−2# (0.059%), and 10−3# (0.062%) into Equation (12), respectively, the calculated lines are shown in Fig. 3. The B contents in the steel and FeO in the slag samples of 10−1# (red dot), 10−2# (green dot), and 10−3# (blue dot) are also presented in Fig. 3.
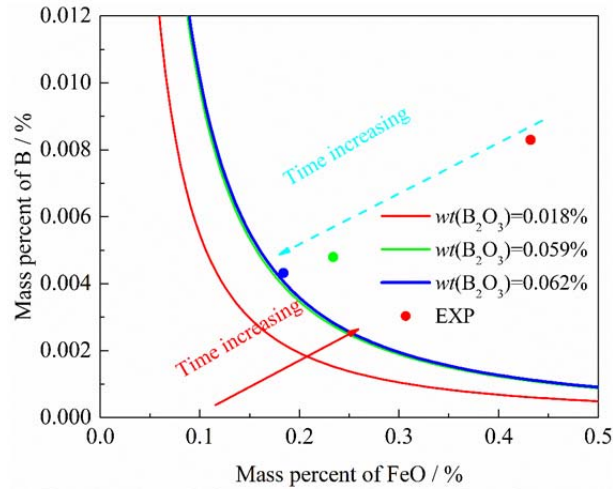
Fig. 3.   The relationship of [B] and (FeO) during the process of 10# heats.

In Fig. 3, with reaction time increasing, the experimental dots moved quickly towards the corresponding theoretical calculation lines. When the reaction time was 60 minute, the 10−3# (blue dot) just fell on the calculated line. The results indicated that the reaction between B and FeO was in equilibrium state at 60 min.

According to the red line in Fig. 3, if the B content in the steel was 0.0083% (the B content in the 10−1# steel sample, red dot), the equilibrium FeO content was 0.064%. It is reasonable to deduce that if the FeO content in the slag of 55%CaF$_2$–20%CaO–3%MgO–22%Al$_2$O$_3$ was as low as 0.064%, the B content can be controlled without any B$_2$O$_3$ addition.

To control the B content even distribution along the ingot, it was necessary to add a certain content of B$_2$O$_3$ into the slag of 55%CaF$_2$–20%CaO–3%MgO–22%Al$_2$O$_3$ for it was difficult to limit the FeO content in the slag as low as 0.064% during the ESR process.

Equation (12) was got by assuming $\Delta G = 0$, for in Fig. 2, the reactions between molten slag and steel were in equilibrium state at 60min. Substitution the equilibrium B$_2$O$_3$ contents in the slag samples of 10−3# (0.062%), 11−3# (0.43%), 12−3# (0.54%), 13−3# (0.81%), and 14−3# (1.13%) into Equation (12), respectively, the calculated equilibrium lines are shown in Fig. 4. The corresponding equilibrium contents of B in the steel and FeO in the slag are also shown in Fig. 4.
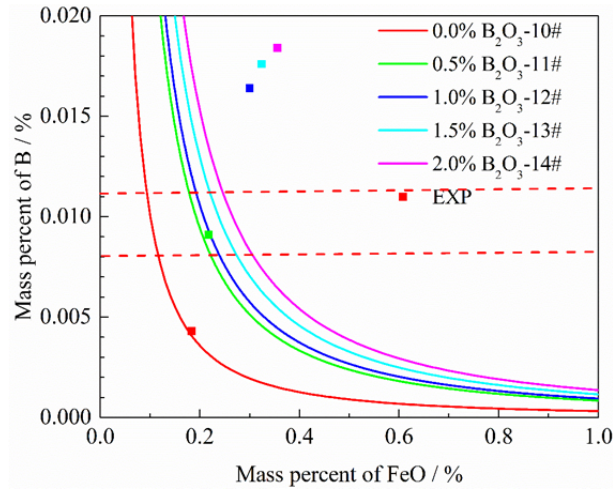
Fig. 4.   The relationship of equilibrium content of B and the content of FeO and B_2O_3 in slag.

In Fig. 4, the experimental dots of the 10−3# and 11−3# fell on the calculated equilibrium lines, while the experimental dots of 12−3#, 13−3#, and 14−3# were far away from the calculated line. The reason was that in the 10# and 11# heats, the reaction between B and FeO occurred and was in equilibrium state at 60 minutes, while in 12#~14# heats, the reaction between B and FeO didn't occur. In 12#~14# heats, B_2O_3 was reduced by the chemically active alloyed element such as Si. To control the B content within the target range, the FeO and B_2O_3 contents in the slag of 55%CaF_2–20%CaO–3%MgO–22%Al_2O_3 should be controlled properly.

When the content of B_2O_3 added into the slag of 55%CaF_2–20%CaO–3%MgO–22%Al_2O_3 is 0.5% (the green line in Fig. 4) and the FeO content ranges from 0.018% to 0.022%, the B content can be controlled within the target range (the dotted line in Fig. 4) with a slight loss.

(3) Analysis of the reaction between Si and B_2O_3

When the content of B_2O_3 added into the slag of 55%CaF_2–20%CaO–3%MgO–

13

22%Al_2O_3 was ≥ 1% (12#~15# heats), the B content increased with the reaction time, and the

Si content decreased concurrently. The reaction between Si and B_2O_3 may occur [22].

$$3[Si]+2(B_2O_3)=4[B]+3(SiO_2) \tag{13}$$

$$\Delta G^{\ominus} = -97920 + 91.2T \tag{14}$$

$$\lg K = \frac{5116.3}{T} - 4.765 \tag{15}$$

$$\Delta G = \Delta G^{\ominus} + RT\ln(\frac{a_B^4}{a_{Si}^3} \times \frac{a_{SiO_2}^3}{a_{B_2O_3}^2}) \tag{16}$$

$$\lg\frac{[B]^4}{[Si]^3} = \lg\frac{(\%B_2O_3)^2}{(\%SiO_2)^3} + \lg\frac{\gamma_{B_2O_3}^2}{\gamma_{SiO_2}^3} + \lg\frac{f_{Si}^3}{f_B^4} + \frac{5113.9}{T} - 4.763 \tag{17}$$

Substitution the known data into the Equation (16), ΔG was negative. The reaction

between Si and B_2O_3 occurred during the experiments process. The calculated line of

Equation (17) is shown in Fig. 5. The corresponding experimental results of the 12#~15#

heats, and the fitting lines of the experimental results are also shown in Fig. 5.
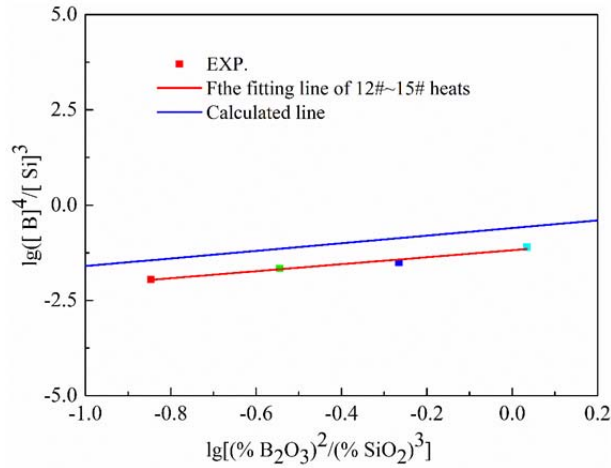
Fig. 5.   The relationship of lg (($\%B_2O_3)^2/(\%SiO_2)^3$) and lg ($[B]^4/[Si]^3$) in 12#~15# heats.

In Fig. 5, the experimental results showed a good linearization tendency. The slope of the

fitting line of the experimental results of 12#~15# heats was equal to the slope of the

calculated line. Based on Fig. 5, the Si content in electrode, and the SiO_2 and B_2O_3 contents

added into the slag of 55%CaF$_2$–20%CaO–3%MgO–22%Al$_2$O$_3$ can be optimized to control the content of m B within the target range.

(4) Analysis of the reaction between Si and Al$_2$O$_3$

The Al content increased with the reaction time in all the six heats, and the Si content decreased concurrently. The reaction between Si and Al$_2$O$_3$ [23] may occur.

$$3[Si]+2(Al_2O_3)=3(SiO_2)+4[Al] \qquad (18)$$

$$\Delta G^{\ominus} = 624680 - 127.8T \qquad (19)$$

$$\Delta G = \Delta G^{\ominus} + RT \ln(\frac{a_{Al}^4}{a_{Si}^3} \times \frac{a_{SiO_2}^3}{a_{Al_2O_3}^2}) \qquad (20)$$

$$\lg\frac{[\%Al]^4}{[\%Si]^3} = \lg\frac{(\%Al_2O_3)^2}{(\%SiO_2)^3} - \lg\frac{f_{Al}^4}{f_{Si}^3} - \lg\frac{\gamma_{SiO_2}^3}{\gamma_{Al_2O_3}^2} - \frac{32639}{T} + 6.67 \qquad (21)$$

Substitution the known data into Equation (20), ΔG was negative. The reaction between Si and Al$_2$O$_3$ occurred. The calculated line of Equation (21) and the corresponding experimental results of the six heats, and the fitting line of the experimental results are shown in Fig. 6.
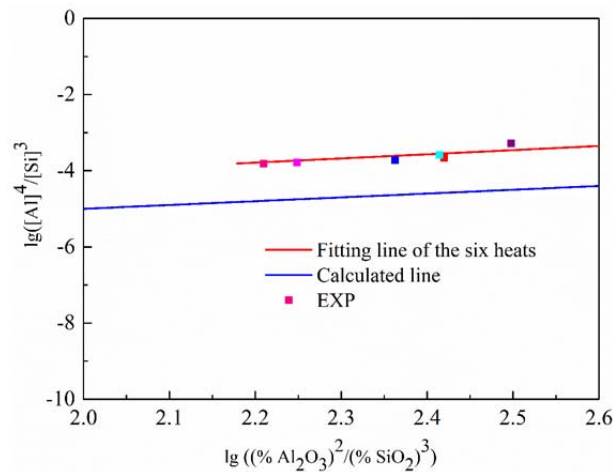
Fig. 6.　The relationship between lg ((%Al$_2$O$_3$)^2/(%SiO$_2$)^3) and lg ([Al]^4/[Si]^3) of each heat.

In Fig. 6, the experimental results showed a good linearization tendency. The slope of the

fitting line was equal to the slope of the calculated line. Based on Fig. 6, the SiO_2 content added into the slag of $55\%CaF_2$–$20\%CaO$–$3\%MgO$–$22\%Al_2O_3$ can be optimized to control the contents of Al and Si within the target range.

(5) Analysis of the reaction between Si and FeO

During the 11# heat, the loss of Si content caused by the reaction between Si and Al_2O_3 was a little, but the loss of equilibrium Si content significantly increased compared with the 10# heat. The reaction between Si and FeO may occur [25].

$$[Si]+2(FeO)=2[Fe]+(SiO_2) \tag{22}$$

$$\Delta G^{\ominus} = -229105.214 + 56.19T \tag{23}$$

$$\Delta G = -229105.214 + 56.19T + RT \ln \frac{a_{[Fe]}^2 \times a_{SiO_2}}{a_{FeO}^2 \times a_{[Si]}} \tag{24}$$

$$\lg[\%Si]=\lg \frac{(\%SiO_2)}{(\%FeO)^2}+\lg \frac{\gamma_{SiO_2}}{\gamma_{FeO}^2}-\lg f_{Si}-3.634 \tag{25}$$

Substitution the known data ($a_{Fe}=1$) into Equation (24), ΔG was negative. Substitution the SiO_2 content in the slag samples of 11−1# (0.84%), 11−2# (1.16%), and 11−3# (1.20%) into Equation (25), respectively, the calculated lines are shown in Fig. 7. The contents of Si in the steel and FeO in the slag samples of 11−1# (red dot), 11−2# (green dot) and 11−3# (blue dot) are also shown in Fig. 7.
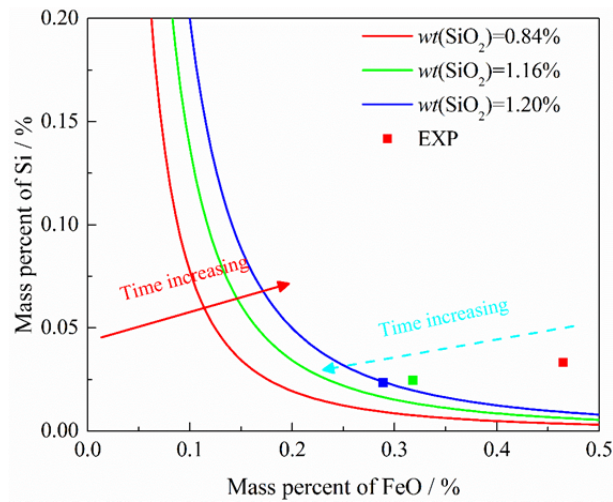
Fig. 7. The relationship between [Si] and (FeO) during the process of 11# heats.

In Fig. 7, with the reaction time increasing, the experimental dots moved quickly towards the corresponding theoretical calculation line. When the reaction time was 60 min, the experimental dot of 11−3# (blue dot) fell on the calculated line. The results indicated that the reaction between Si and FeO was in equilibrium state at 60 min. The Si content reduced quickly at the first 20 min. To control the Si content even distribution along the ingot, a certain content of SiO_2 should be added into the slag of 55%CaF_2–20%CaO–3%MgO–22%Al_2O_3, and the *wt* (FeO) in the slag should also be limited.

(6) Analysis of the content of O in the steel

The O content decreased with the reaction time in each heat, but the equilibrium O contents at 60 min of the six heats increased with B_2O_3 content increasing (shown in Fig. 2). The equilibrium O content in steel was determined by the [M] × [O] [26] (M is the alloyed element).

The affinity between O and Al was stronger than the affinity between O and Si, the analysis of the relationship between Al and O was shown below [25−26].

17

$$(Al_2O_3) = 2[Al] + 3[O] \tag{26}$$

$$\lg K = -\frac{64000}{T} + 20.57 \tag{27}$$

$$[O] = \left(\frac{a_{Al_2O_3} \times K}{f_{Al}^2 \times f_O^3}\right)^{1/3} \times \frac{1}{[Al]^{2/3}} \tag{28}$$

Substitution the known data into Equation(28), the calculated line of Equation (28) and the equilibrium contents of Al and O in the six heats are shown in Fig. 8 (for the constant terms in Equation (28) are close, the different calculated lines are almost coincident, only one line is shown here).
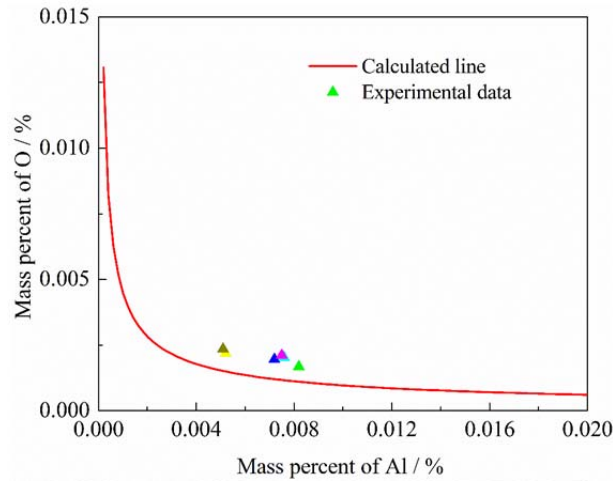
Fig. 8.   The relationship between the equilibrium content of O and Al.

In Fig. 8, the experimental data was around the calculated line. It was deduced that the O content was controlled by Al content in steel and the oxidation product was Al_2O_3. To reduce the degree of the reaction between Si and Al_2O_3 and inhibit the formation of the detrimental oxidation product of Al_2O_3, a certain content of SiO_2 should be added into the slag of 55%CaF$_2$–20%CaO–3%MgO–22%Al$_2$O$_3$.

4 Conclusions

The principal conclusions concluded from this study are summarized as follows:

1) When the B_2O_3 content added into the slag of 55%CaF_2–20%CaO–3%MgO–22%Al_2O_3 is 0.5% (wt%) and the content of FeO in the molten slag ranges from 0.18% to 0.22%, the B content in the steel can be controlled within the narrow target range with a slight loss.

2) When the B_2O_3 content added into the slag of 55%CaF_2–20%CaO–3%MgO–22%Al_2O_3 is ≥ 1% (wt%), the reaction between Si and B_2O_3 leads to the increasement of B content. The proper B_2O_3 and SiO_2 contents added into the slag of 55%CaF_2–20%CaO–3%MgO–22%Al_2O_3 should be based on the ratio of [B] / [Si] in the electrode.

3) A certain content of SiO_2 should be added into the slag of 55%CaF_2–20%CaO–3%MgO–22%Al_2O_3 (wt%) to reduce the degree of the reaction between Si and Al_2O_3, and the proper additional content of SiO_2 should be based on the Si content in the electrode and the Al_2O_3 content in the slag.

Acknowledgements

Conflicts of Interest

The author declare that we do not have any commercial or associative interest that represents a conflict of interest in connection with the work submitted.

中图分类号：TF142

二级学科名称：钢铁冶金

Reference

[1] Y.Y. Yang, L.G. Wang, C.Q. Dong, G. Xu, T. Morosukbm, and G. Tsatsaronisb, Comprehensive exergy-based evaluation and parametric study of a coal-fired ultra-supercritical power plant, *Appl. Energ.* 112(2013), p. 1087.

[2] J.P. Ciferno, T.E. Fout, A.P. Jones, and J.T. Murphy, Capturing carbon from existing coal-fired power plants, *Chem. Eng. Prog.*, 105*(*2009*)*, No. 4, p. 33.

[3] Y. Zeng, J. Jia, W. Cai, S. Dong and Z. Wang, Effect of long-term service on the precipitates in P92 steel, *Int. J. Min. Met. Mater.*, 25(2018), No. 8, p. 913.

[4] F. Abe, T. Horiuchi, M. Taneike, and K. Sawada, Stabilization of martensitic microstructure in advanced 9Cr steel during creep at high temperature, *Mat. Sci. Eng. A* 378(2004), No. 1-2, p. 299.

[5] P.J. Maziasz. Developing an austenitic stainless steel for improved performance in advanced fossil power facilities, *JOM*, 41(1989), No. 7, p. 14.

[6] N. Blaes, B. Donth, and D. Bokelmann, High chromium steel forgings for steam turbines at elevated temperatures, *Energy. Mater.*, 2(2007), No. 4, p. 207.

[7] H. Chalmers and J. Gibbins, Initial evaluation of the impact of post-combustion capture of carbon dioxide on supercritical pulverised coal power plant part load performance, *Fuel*, 86(2007), No. 14, p. 2109.

[8] R. Viswanathan and W. Bakker, Materials for ultra-supercritical coal power plants—Turbine materials: Part II, *J. Mater. Eng. Perform.*10(2001), No. 1, p. 96.

[9] V. Weber, A. Jardy, B. Dussoubs, D. Ablitzer, S. Rybéron, V. Schmitt, S. Hans, and H. Poisson, A comprehensive model of the electroslag remelting process: description and validation, *Metall. Mater. Trans. B*, 40(2009), No. 3, p. 271.

[10] Y. Dong, Z. Jiang, H. Liu, R. Chen, and Z. Song, Simulation of multi-electrode ESR process for manufacturing large ingot. *ISIJ int.*, 52(2012), No. 12, p. 2226.

[11] S.S. Kasana and O. P. Pandey, Effect of electroslag remelting and homogenization on hydrogen flaking in AMS-4340 ultra-high-strength steels, *Int. J. Min. Met. Mater.*, 26(2019), No. 5, p. 611.

[12] E. Plockinger, *The Hatfield Memorial Lectures*, Vol. 3, CRC Press, Boca Raton, 2005, p. 45.

[13] J.A.V.D. Avyle, J.A. Brooks, and A.C. Powell, Reducing defects in remelting processes for high-performance alloys, *JOM*, 50(1998), No. 3. p. 22.

[14] S.J. Li, G.G. Cheng, Z.Q. Miao, L. Chen and X.Y. Jiang, Effect of slag on oxide inclusions in carburized bearing steel during industrial electroslag remelting, *Int. J. Min. Met. Mater.*, 26(2019), No. 3, p. 291.

[15] V. Knežević, J. Balun, G. Sauthoff, G. Inden, and A. Schneider, Design of martensitic/ferritic heat-resistant steels for application at 650℃ with supporting thermodynamic modelling, *Mat. Sci. Eng. A-Struct.*, 477(2008), No. 1-2, p. 334.

[16] F. Masuyama, History of power plants and progress in heat resistant steels, *ISIJ Int.*,

41(2001), No. 6, p. 612.

[17] T. Ishitsuka, Y. Inoue, and H.Ogawa, Effect of silicon on the steam oxidation resistance of a 9% Cr heat resistant steel, *Oxid. Met.*, 61(2004), No. 1-2, p. 125.

[18] A. Mitchell, F. Reyes-Carmona, and E. Samuelsson, The deoxidation of low-alloy steel ingots during ESR, *ISIJ Int.* 24(1984), No. 7, p. 547.

[19] F. Reyes-Carmona and A. Mitchell, Deoxidation of ESR slags, *ISIJ Int.* 32(1992), No. 4, p. 529.

[20] G. Pateisky, H. Biele, and H.J. Fleischer, The Reactions of Titanium and Silicon with Al_2O_3-CaO-CaF_2 Slags in the ESR Process, *J. Vac. Sci. Technol.* 9(1972), No. 6, p. 1318.

[21] S.F. Medina and A. Cores, Thermodynamic aspects in the manufacturing of micro-alloyed steels by the electroslag remelting process, *ISIJ int.*, 33(1993), No. 12, p. 1244.

[22] J. Fedko and M. Krucinski, Thermodynamic analysis of boron concentration changes in steel during electroslag remelting, *Ironmak. Steelmak.,* 16(1989), No. 2, p. 116.

[23] D.S. Kim, G.J. Lee, M.B. Lee, J.I. Hur, and J.W. Lee, Manufacturing of 9CrMoCoB Steel of Large Ingot with Homogeneity by ESR Process, *IOP Conf. Series: Mater. Sci. Eng.*, 143(2016), No. 1, p. 012002.

[24] V.A. Grigorân, L.N. Belânčikov, and A.Â. Stomahin, *Theoretical principles of electric steelmaking,* Mir Publishers, Milpitas, 1983, p. 154.

[25] Y.J. Liang, Y.C. Che, and X.X. Liu, *Thermodynamics data book*, Northeast University Press, Shenyang, 1993, p. 216.

[26] X.H. Huang, *Principles of Iron and Steel Metallurgy*, Metallurgical Industry Press, Beijing, 1981, p. 309.